JOURNAL OF AIRCRAFT
Vol. 40, No. 4, July–August 2003

Numerical Simulation of Inviscid Incompressible Two-Dimensional Airfoil–Vortex Interaction in Ground Effect

Gustavo F. Fonseca* and Gustavo C. R. Bodstein†
Federal University of Rio de Janeiro, 21945-970 Rio de Janeiro, Brazil
and
Miguel H. Hirata‡
Federal University of Itajuba, 37500-000 Itajuba, Brazil

A numerical inviscid vortex method is employed to study the unsteady, two-dimensional, incompressible flow that occurs during an airfoil–vortex interaction in the vicinity of a ground plane. The airfoil bound vorticity is modeled using a panel method with linear piecewise-continuous vorticity distribution. The vortex is considered to be a point vortex, and the ground effect is obtained using the method of images. Point vortices are also generated at the airfoil trailing edge to ensure that circulation is conserved and that the Kutta condition is satisfied. All vortices are convected using a first-order Lagrangian time-marching scheme. After code validation, numerical results for the airfoil–vortex interaction in ground effect reveal that the loading on the airfoil is affected by the thickness, angle of attack, and height of the airfoil above the ground, as well as the vortex strength, direction of rotation, and distance to the airfoil. The wake evolution is nonlinear and strongly influenced by the interaction, whereas the pressure distribution on the ground presents steep adverse gradients.

Nomenclature

A, B	=	influence coefficient matrices
C_a	=	airfoil contour
C_l, C_m	=	lift and pitching moment coefficients
C_p	=	pressure coefficient
c	=	airfoil chord
H	=	minimum airfoil–vortex height
h	=	height of the airfoil to the ground
h_g	=	chord-to-wall clearance ratio
h_v	=	dimensionless H
K	=	interaction parameter
K_a	=	apparent interaction parameter
l	=	lift force
M	=	number of time steps
m	=	pitching moment
N	=	number of panels on airfoil surface
$\boldsymbol{n}$	=	unit normal vector
P	=	path of integration
p	=	pressure field
S	=	panel length
s	=	tangential coordinate
$\boldsymbol{s}$	=	unit tangential vector
t, Δt	=	time and time-step
U_∞	=	freestream speed of uniform flow
u, v	=	horizontal and vertical components of $\boldsymbol{u}$
$\boldsymbol{u}$	=	velocity field
x, y	=	horizontal and vertical components of $\boldsymbol{x}$
$\boldsymbol{x}$	=	Cartesian coordinate
α	=	angle of attack
β	=	extra panel angle with the x axis
Γ	=	vortex strength
γ	=	vorticity per unit length
ε	=	airfoil thickness
θ	=	airfoil panel angle with the x axis
ρ	=	fluid density
ϕ	=	velocity potential
ω	=	vorticity field

Subscripts

a	=	airfoil surface
g	=	ground surface
i, j, k	=	summation indexes
im	=	image
l	=	lower
te	=	trailing edge
u	=	upper
v	=	main vortex
w	=	wake
0	=	initial condition
∞	=	freestream flow

Introduction

The study of the unsteady, incompressible, two-dimensional flow resulting from airfoil–vortex interaction in ground effect (AVIG) finds application in many engineering problems. Short thin plates, known as large-eddy breakup devices (LEBUs) or flow manipulators, are placed in a turbulent boundary layer above a large plane wall to reduce the drag per unit area on the wall. The reduction in drag per unit area persists downstream of the plate, as confirmed by experiments.[1,2] On the other hand, the effect of vorticity disturbances passing around an airfoil in the vicinity of a wall causes fluctuating aerodynamic forces on both the airfoil and the wall. If the vorticity disturbance is idealized as a free two-dimensional moving vortex, the interaction changes the vortex trajectory, which feedbacks the interaction again. As pointed out by Gebert and Atassi,[3] the understanding of AVIG flows also applies to structures in ground transportation or on the top of buildings subject to atmospheric turbulence, ships in restricted waters, and wings during takeoff and landing. In this latter case, the flow around a wing in ground effect craft[4] is strongly affected by the interaction with an oncoming vortex. Panaras[5] cites the flow inside a turbomachine as one of his motivations to devise a numerical model of blade–vortex interaction.

Received 7 November 2000; revision received 13 February 2003; accepted for publication 10 March 2003. Copyright © 2003 by the American Institute of Aeronautics and Astronautics, Inc. All rights reserved. Copies of this paper may be made for personal or internal use, on condition that the copier pay the $10.00 per-copy fee to the Copyright Clearance Center, Inc., 222 Rosewood Drive, Danvers, MA 01923; include the code 0021-8669/03 $10.00 in correspondence with the CCC.

*Graduate Student, Department of Mechanical Engineering—EE/COPPE, C. P. 68503.
†Associate Professor, Department of Mechanical Engineering—EE/COPPE, C. P. 68503. Senior Member AIAA.
‡Visiting Professor, Department of Mechanics—IEM, C. P. 50.

This flow is characterized by the interaction of vortices generated upstream with a rotor blade, generally occurring in close proximity to the turbomachine casing, which can be modeled as a large wall. Despite the flow complexities, a two-dimensional inviscid model is able to capture most of the important phenomena that take place in the real flow.

The AVIG flow may be thought of as a combination of three flows: airfoil–vortex interaction (AVI), airfoil–ground interaction (AGI), and vortex–ground interaction (VGI). A large number of papers on the unsteady, incompressible, two-dimensional AVI flow have been published. Within the context of the (two-dimensional) parallel AVI that occurs around helicopter rotors, known as blade–vortex interaction (BVI), Panaras,[5] Poling et al.,[6] and Lee and Smith,[7] among others, have devised numerical models based on the inviscid discrete vortex method coupled with linearized potential flow theory or panel methods. More elaborate numerical models have also been employed, such as those based on Euler (see Ref. 8) and Navier–Stokes (see Ref. 9) mesh-based methods. Detailed experimental investigations on the aerodynamics of parallel BVI have been performed by Seath et al.,[10] Straus et al.[11] and Chen and Chang.[12] See the review articles of McCune and Tavares[13] and Mook and Dong[14] for additional references on unsteady, incompressible flows over airfoils and the numerical simulation of wakes and BVI.

The steady potential flow around a thin airfoil in ground effect, the AGI flow, has been treated analytically by Havelock[15] and Green.[16] Widnall and Barrows[17] find an analytical solution using thin-airfoil theory and the method of asymptotic expansions for small airfoil thickness, angle of attack, and chord-to-wall clearance ratio. Similarly, Plotkin and Kennell[18] obtain an asymptotic series for small values of the airfoil thickness and angle of attack, but for large values of the chord-to-wall clearance ratio. Dragos[19] integrates numerically the thin-airfoil equation using Gauss-type quadrature formulas, but the solution is also valid for large chord-to-wall clearance ratios. More recently, Coulliette and Plotkin[20] revisit the airfoil in ground effect problem, both analytically and numerically, and obtain analytical solutions based on asymptotic series valid near and far from the ground and numerical results using a linear vortex panel method. Colliette and Plotkin show that, for small values of camber and angle of attack, normalized lift is enhanced near the ground and reduced far from it, whereas for a fixed distance above the ground, normalized lift decreases with increasing angle of attack and camber. Thickness reduces lift at all heights above the ground.

The interaction of a vortex and a ground plane, the VGI flow, has also been extensively studied in the literature. The inviscid interaction of a point vortex and a wall can be easily treated by potential flow theory with the aid of complex variable theory and the method of images, as shown by Milne-Thomson.[21] This flow is characterized by a strong suction peak underneath the vortex, as seen from an observer fixed to the vortex center. In a viscous flow, this pressure distribution may cause flow separation in the wall boundary layer, depending on the vortex strength and vortex distance to ground. This so called vortex-induced separation causes the boundary-layer fluid on the upgoing side of the vortex to erupt into the irrotational flow, changing the entire flowfield. Viscous vortex–wall interactions have been treated numerically by many authors, and a very comprehensive review of these articles can be found by Doligalski et al.[22]

For the more complex AVIG flow, which combines all three problems, not many theoretical works have been developed. In the context of LEBU devices, Dowling[23] uses linearized potential flow theory to analyze the passage of a point vortex over a splitter plate. In the model problem, the flow around a thin flat plate in ground effect is perturbed by an oncoming line vortex. Balakumar and Widnall[24] also use potential flow theory to treat analytically the unsteady, two-dimensional, inviscid and incompressible flow around a thin flat plate immersed in a sinusoidal vortical disturbance in ground effect. Also employing potential flow theory, Gerbert and Atassi[3] use Sears functions to study the same two-dimensional problem and focus their analysis on the dependence of the fluctuating lift and velocity field on the frequency of the vortical disturbance. It is clear that important aspects of AVIG flows have not yet been accounted for in the literature, such as the effect of the geometrical parameters, angle of attack, and the nonlinear wake interaction on the flow as a whole.

Thus, we propose a more elaborate numerical model to simulate the interaction of an airfoil and a vortex in ground effect. Our model is an extension of the one developed by Fonseca et al.[25] to study the AVI flow. We employ a linear, piecewise-continuous vortex panel method to discretize the airfoil bound vorticity, whose strength is found by enforcing the impermeability condition on the airfoil control points. The Kutta condition is imposed through the continuity of the pressure field at the airfoil trailing edge, combined with Kelvin's circulation theorem; this procedure provides a model for the vortex shedding mechanism at the trailing edge, responsible for the injection of vorticity into the wake. The main vortex that interacts with the airfoil and the vorticity in the wake are modeled as two-dimensional point vortices. All of the vortices in the flow are convected using a first-order Lagrangian time-marching scheme. We present results for the aerodynamic loadings on the airfoil and the ground, as well as for the wake configuration during the AVIG flow.

Mathematical Model

We consider a two-dimensional airfoil with chord c immersed in a uniform flow with freestream speed U_∞ undergoing a parallel interaction with a main vortex above the ground. The airfoil is placed a height h above the ground (from the leading edge) and is set at an angle of attack α. All variables in the analysis that follows are nondimensionalized by U_∞ and c. The vortex has constant dimensionless strength Γ_v (clockwise rotation considered positive), which occupies the position $[x_v(t), y_v(t)]$ at time t. The ground is viewed as an infinite plane wall. Figure 1 shows the flow geometry and the Cartesian coordinate system used. We assume the flow to be two dimensional, unsteady, incompressible, and inviscid. For this flow, the velocity field must satisfy the continuity and Euler equations and the associated boundary conditions.

In the fluid region,

$$\nabla \cdot \boldsymbol{u} = 0 \tag{1}$$

In the fluid region,

$$\frac{\partial \boldsymbol{u}}{\partial t} + \boldsymbol{u} \cdot \nabla \boldsymbol{u} = -\nabla p \tag{2}$$

On the airfoil surface,

$$\boldsymbol{u} \cdot \boldsymbol{n}_a = 0 \tag{3a}$$

On the ground surface,

$$\boldsymbol{u} \cdot \boldsymbol{n}_g = 0 \tag{3b}$$

At infinity,

$$|\boldsymbol{u}| \to 1 \tag{3c}$$

The real flow has nonzero vorticity in the core of the main vortex, in the airfoil and ground boundary layers, and in the airfoil wake. We model the main vortex as a point vortex and the wake as an array of point vortices. The airfoil boundary layer is lumped into the bound vorticity attached to the airfoil surface, and we disregard the boundary layer on the ground. Thus, our flow is rotational, and

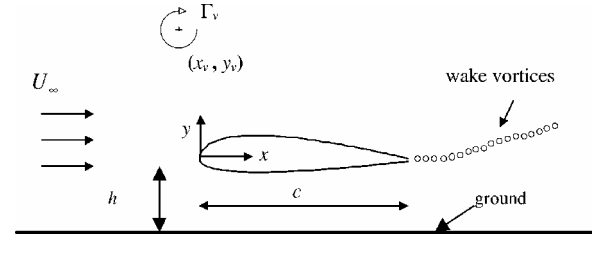

Fig. 1 Schematic of the flow geometry.

we use the inviscid vorticity transport equation, which can be written as

$$\frac{\mathrm{D}\omega}{\mathrm{D}t} \equiv \left(\frac{\partial}{\partial t} + \boldsymbol{u} \cdot \nabla\right)\omega = 0 \tag{4}$$

In a two-dimensional flow, ω is the only nonzero component of the vorticity vector, namely, the component normal to the plane of the flow, and, therefore, is a scalar quantity. In a Lagrangian representation, Eq. (4) states that the rate of change of ω following a fluid particle is zero, and the vorticity moves with the fluid. This allows us to use a Lagrangian time-marching scheme to convect each point vortex by solving the system of ordinary differential equations (ODEs) for their positions,

$$\frac{\mathrm{d}\boldsymbol{x}_v}{\mathrm{d}t} = \boldsymbol{u}_v[\boldsymbol{x}_v(t), t] \tag{5}$$

The airfoil boundary layer is accounted for by integrating the vorticity over the boundary layer, in the limit as its thickness goes to zero. It can be shown[13] that the airfoil bound vorticity per unit length γ distributed along the airfoil surface is given by

$$\gamma(s, t) = \boldsymbol{u} \cdot \boldsymbol{s}_a \tag{6}$$

Away from the airfoil surface and the points occupied by the main and wake vortices, the flow is irrotational, and we can write Eqs. (1) and (3) in terms of the velocity potential ϕ as follows.

In the fluid region,

$$\nabla^2\phi = 0 \tag{7a}$$

On the airfoil surface,

$$\nabla\phi \cdot \boldsymbol{n}_a = 0 \tag{7b}$$

On the ground surface,

$$\nabla\phi \cdot \boldsymbol{n}_g = 0 \tag{7c}$$

At infinity,

$$|\nabla\phi| \to 1 \tag{7d}$$

Because of the linearity of the boundary-value problem (7), ϕ can be written as a superposition of solutions in the form

$$\phi = \phi_\infty + \phi_v + \phi_a + \phi_w + \phi_g \tag{8}$$

so that each contribution on the right-hand side of Eq. (8) satisfies Laplace's equation (7a). The freestream and the main vortex velocity potentials are given, respectively, by

$$\phi_\infty = x \tag{9a}$$

$$\phi_v = \frac{\Gamma_v}{2\pi}\tan^{-1}\left[\frac{y - y_v(t)}{x - x_v(t)}\right] \tag{9b}$$

The airfoil velocity potential due to the bound vorticity on the airfoil surface is found using the vortex panel method, where the airfoil contour is discretized into N small straight panels with vorticity distributed along the panel length. Thus, ϕ_a can be written as

$$\phi_a = \frac{1}{2\pi}\sum_{i=1}^{N}\int_{S_i}\gamma_i(s_i, t)\tan^{-1}\left[\frac{y - y_i(s_i, \theta_i)}{x - x_i(s_i, \theta_i)}\right]\mathrm{d}s \tag{9c}$$

The wake velocity potential comprises two terms: one corresponding to $(M-1)$ point vortices generated at previous times $t_1, \ldots, t_{M-1}$ and the other due to the amount of vorticity $\Delta\Gamma_w$ shed at time t_M from the airfoil trailing edge. We model $\Delta\Gamma_w$ as an extra panel with constant vorticity distribution per unit arc length γ_w and length S_w, where $\Delta\Gamma_w = \gamma_w S_w$. At time t_{M+1}, the extra panel is transformed into a discrete vortex with strength $\Gamma_w = \Delta\Gamma_w$, and a new extra panel is created. Hence, ϕ_w at t_M can be written as

$$\phi_w = -\frac{1}{2}\gamma_w\int_{S_w}\tan^{-1}\left[\frac{y - y_w(s_w, \theta_w, t)}{x - x_w(s_w, \theta_w, t)}\right]\mathrm{d}s + \sum_{k=1}^{M-1}\frac{\Gamma_{w,k}}{2\pi}\tan^{-1}\left[\frac{y - y_{w,k}(t)}{x - x_{w,k}(t)}\right] \tag{9d}$$

The effect of the ground plane on the flow may be taken into account using the method of images, which consists of adding a reflected flow (with respect to the x axis) to the original flow. Thus, the ground velocity potential ϕ_g is expressed as a sum of the mirror images of the main vortex, the airfoil, and the wake potentials, that is,

$$\phi_g = \phi_{v,\mathrm{im}} + \phi_{a,\mathrm{im}} + \phi_{w,\mathrm{im}} \tag{9e}$$

Reflection with respect to the x axis means that the signs of all of the vortex strengths must be changed, and their positions (x_v, y_v) in Eqs. (9b–9d) must be replaced by $(x_{v,\mathrm{im}}, y_{v,\mathrm{im}})$, where $x_{v,\mathrm{im}} = x_v$, $y_{v,\mathrm{im}} = -(y_v + 2h_g)$, and the chord-to-wall ratio is defined as $h_g = h/c$. Equations (9b–9e) individually vanish at infinity and, therefore, do not affect the boundary condition (7d), which is satisfied by Eq. (9a). Also, with the inclusion of Eq. (9e), the boundary condition (7c) is automatically satisfied for all times. It remains to enforce boundary condition (7b) on the airfoil to determine the unknown ϕ_a (and its image). Using Eqs. (8) and (9e), we write Eq. (7b) as

$$(\nabla\phi_a + \nabla\phi_v + \nabla\phi_w + \nabla\phi_{a,\mathrm{im}} + \nabla\phi_{v,\mathrm{im}} + \nabla\phi_{w,\mathrm{im}} + \nabla\phi_\infty) \cdot \boldsymbol{n}_a = 0 \tag{10}$$

For the solution to be unique, the Kutta condition needs to be imposed, which requires the continuity of pressure across the airfoil trailing edge. The unsteady Bernoulli equation, obtained from integration of the Euler equations (2), can be written for the pressure coefficient C_p as

$$C_p \equiv \frac{p - p_\infty}{1/2\rho U_\infty^2} = 1 - \boldsymbol{u} \cdot \boldsymbol{u} - 2\frac{\partial\phi}{\partial t} = 1 - \nabla\phi \cdot \nabla\phi - 2\frac{\mathrm{d}}{\mathrm{d}t}\int_P \nabla\phi \cdot \mathrm{d}\boldsymbol{s} \tag{11}$$

The path P is taken from a point far upstream from the leading edge to a point on the airfoil surface. Evaluating Eq. (11) at the upper and lower surfaces of the trailing edge and applying the Kutta condition, we have

$$\frac{\mathrm{d}}{\mathrm{d}t}(\phi_{u,\mathrm{te}} - \phi_{l,\mathrm{te}}) = \frac{1}{2}(\nabla\phi_{l,\mathrm{te}} \cdot \nabla\phi_{l,\mathrm{te}} - \nabla\phi_{u,\mathrm{te}} \cdot \nabla\phi_{u,\mathrm{te}}) \tag{12}$$

The quantity $(\phi_{u,\mathrm{te}} - \phi_{l,\mathrm{te}})$ is related to the circulation Γ_a around a contour C_a that encloses only the airfoil via the following equation:

$$\Gamma_a(t) \equiv \oint_{C_a}\boldsymbol{u} \cdot \mathrm{d}\boldsymbol{s} = \oint_{C_a}\nabla\phi \cdot \mathrm{d}\boldsymbol{s} = \phi_{u,\mathrm{te}}(t) - \phi_{l,\mathrm{te}}(t) \tag{13}$$

Differentiating Eq. (13) with respect to t and using Eqs. (12) and (6), we obtain

$$\frac{\mathrm{d}\Gamma_a}{\mathrm{d}t} = \frac{1}{2}(\nabla\phi_{l,\mathrm{te}} \cdot \nabla\phi_{l,\mathrm{te}} - \nabla\phi_{u,\mathrm{te}} \cdot \nabla\phi_{u,\mathrm{te}}) = \frac{1}{2}\left(\gamma_{l,\mathrm{te}}^2 - \gamma_{u,\mathrm{te}}^2\right) \tag{14}$$

The variation of Γ_a with time can be written in terms of the dimensionless vortex, airfoil, and wake circulations applying Kelvin's circulation theorem. If the initial circulation in the flow, Γ_0, is given by $\Gamma_0 \equiv \Gamma(t = 0) = \Gamma_v = \mathrm{const}$, which is the initial condition used in the computations, and the total circulation is $\Gamma_v + \Gamma_a(t) + \Gamma_w(t) = \Gamma_0$, then we can write

$$\frac{\mathrm{d}\Gamma_a}{\mathrm{d}t} = -\frac{\mathrm{d}\Gamma_w}{\mathrm{d}t} \tag{15}$$

which determines the amount of vorticity shed at the trailing edge and, therefore, provides a model for the generation of the vorticity that forms the wake.

With Eq. (11), the lift and pitching moment coefficients are given, respectively, by

$$C_l \equiv \frac{l}{(1/2)\rho U_\infty^2 c} = \oint_{C_a} \gamma^2(s,t)\sin\theta(s)\,\mathrm{d}s + 2\frac{\mathrm{d}}{\mathrm{d}t}\oint_{C_a}\sin\theta(s)\int_0^s \gamma(\xi,t)\,\mathrm{d}\xi\,\mathrm{d}s \tag{16a}$$

$$C_m \equiv \frac{m}{(1/2)\rho U_\infty^2 c^2} = \oint_{C_a} \gamma^2(s,t)x(s)\sin\theta(s)\,\mathrm{d}s - \oint_{C_a}\gamma^2(s,t)y(s)\cos\theta(s)\,\mathrm{d}s + 2\frac{\mathrm{d}}{\mathrm{d}t}\oint_{C_a} x(s)\sin\theta(s) \times \int_0^s \gamma(\xi,t)\mathrm{d}\xi\,\mathrm{d}s - 2\frac{\mathrm{d}}{\mathrm{d}t}\oint_{C_a} y(s)\cos\theta(s)\int_0^s \gamma(\xi,t)\,\mathrm{d}\xi\,\mathrm{d}s \tag{16b}$$

The lower limit of integration in the innermost integrals corresponds to the lower trailing edge. The moment is positive in the clockwise direction and is calculated about the leading edge.

Numerical Scheme

The airfoil velocity potential ϕ_a is calculated using a vortex panel method. The airfoil contour is discretized into N small panels, with a higher concentration of panels in the neighborhood of the leading and trailing edges. Each panel has a linear distribution of vorticity along its length in the form $\gamma_i(s_i) = \gamma_i + (\gamma_{i+1} - \gamma_i)(s_i/S_i)$, so that it is piecewise continuous at the panel endpoints (or nodes). Thus, the integral in Eq. (9c) can be evaluated, and the normal component of the velocity induced by the ith panel at the midpoint (control point) of a jth panel can be written in matrix form as

$$(\nabla\phi_a \cdot \boldsymbol{n})_i = \sum_{j=1}^{N+1} A_{ij}\gamma_j \tag{17}$$

The influence coefficients of Eq. (17) can be found in Mook and Dong[13] or Katz and Plotkin.[26] To write γ_w in terms of γ_1 and γ_{N+1} at the trailing edge, we discretize the Kutta condition given by Eq. (14) in the form

$$\Delta\Gamma_a \equiv \Gamma_a(t_M) - \Gamma_a(t_{M-1}) = \tfrac{1}{2}\Delta t\left(\gamma_{l,\mathrm{te}}^2 - \gamma_{u,\mathrm{te}}^2\right) = (\gamma_{l,\mathrm{te}} - \gamma_{u,\mathrm{te}})\{[(\gamma_{l,\mathrm{te}} + \gamma_{u,\mathrm{te}})/2]\Delta t\} \tag{18}$$

where $\Gamma_a(t)$ is given by

$$\Gamma_a(t) = \frac{1}{2}\sum_{i=1}^{N}(\gamma_i + \gamma_{i+1})S_i$$

From Eq. (18), we use the relations $\gamma_{l,\mathrm{te}} = -\gamma_1$ and $\gamma_{u,\mathrm{te}} = \gamma_{N+1}$ and define γ_w, which is constant along the extra panel, by

$$\gamma_w \equiv (\gamma_{l,\mathrm{te}} - \gamma_{u,\mathrm{te}}) = -(\gamma_1 + \gamma_{N+1}) \tag{19}$$

Equation (15) for the conservation of circulation allows that $\Delta\Gamma_w$ be expressed as

$$\Delta\Gamma_w \equiv \gamma_w S_w = -\Delta\Gamma_a \tag{20}$$

When Eqs. (19) and (20), are used, Eq. (18) can be written as

$$\Delta\Gamma_w = (\gamma_1 + \gamma_{N+1})S_w \tag{21a}$$

where the length of the extra panel is defined as the term in the braces of Eq. (18), that is,

$$S_w \equiv [(\gamma_{N+1} - \gamma_1)/2]\Delta t \tag{21b}$$

The angle between the extra panel and the x axis, β_w, is determined by ensuring that the shed vorticity leaves the trailing edge along a local instantaneous streamline, that is,

$$\beta_w = \tan^{-1}(v_w/u_w) \tag{22}$$

The $(N+1)$ unknown γ_i are now determined from the impermeability boundary condition Eq. (10), which is imposed on the N airfoil control points. With the aid of Eqs. (9) and (21a) the remaining terms of Eq. (10) can be written in matrix form for the ith panel as follows:

$$\sum_{j=1}^{N+1} A_{ij}\gamma_j + (\gamma_1 + \gamma_{N+1})A_{w,i} + B_{v,i}\Gamma_v + \sum_{k=1}^{M-1} B_{w,ik}\Gamma_{w,k} + \sum_{j=1}^{N+1} A_{ij_{\mathrm{im}}}\gamma_j + (\gamma_1 + \gamma_{N+1})A_{w,i_{\mathrm{im}}} + B_{v,i_{\mathrm{im}}}\Gamma_v + \sum_{k=1}^{M-1} B_{w,ik_{\mathrm{im}}}\Gamma_{w,k} + (\nabla\phi_\infty \cdot \boldsymbol{n})_i = 0 \tag{23}$$

$$i = 1, 2, \ldots, N$$

The terms on the left-hand side of Eq. (24) correspond to the airfoil panels, the extra panel, the main vortex, the wake vortices, their images, and the uniform flow, respectively. To render the linear system of algebraic Eqs. (23) determined, which comprise $N+1$ unknowns and only N equations, we include Eqs. (21) and (22), which add the two unknowns S_w and β_w. The computations are performed by iteration so that S_w and β_w are first guessed, yielding a system with $N+1$ equations and $N+1$ unknowns. After the solution is obtained, Eqs. (21b) and (22) are used again to recalculate the values of S_w and β_w. This procedure is repeated until both variables converge.[25] As soon as the computations at time t_M converge, the pressure distribution and the lift and pitching moment coefficients on the airfoil are calculated. The main vortex and the wake vortices are then convected using a first-order Euler time-marching scheme, obtained from a discretization of Eq. (5) in the form

$$\boldsymbol{x}_v(t + \Delta t) = \boldsymbol{x}_v(t) + \boldsymbol{u}_v(\boldsymbol{x}_v, t)\Delta t \tag{24}$$

with initial condition (x_{v0}, y_{v0}) at $t = 0$ for the main vortex (point where the main vortex is released in the flow). The wake extra panel is transformed into a point vortex with strength $\Gamma_w = \Delta\Gamma_w$ and is convected using Eq. (24). At the end of the step, the dimensionless computational time t_M is incremented by Δt, and the entire procedure is repeated.

The loading on the airfoil is obtained by integrating Eqs. (16) numerically. For the computation of the last term on the right-hand side of Eq. (11), the path of integration P starts from $x_\infty = -2x_{v0}$, on the ground surface, proceeds along the ground to $x = 1$, goes straight up to the trailing edge, and follows the airfoil contour up to the desired panel.

Results and Discussion

Code Validation

The numerical algorithm described in the preceding sections is an extension of the mathematical model developed by Fonseca et al.,[25] which, in turn, is inspired by the inviscid vortex method devised by Vezza and Galbraith[27] to study unsteady, two-dimensional, and incompressible flows around an airfoil resulting from a step change in angle of attack, sinusoidal oscillations, and ramp motions. Because this extended algorithm takes into account the effect of the presence of the ground plane through the application of the method of images, it changes neither the time-stepping integration scheme of the

ODE system nor the airfoil panel discretization technique. Therefore, the modified code is still asymptotically first order in time and second order in the number of panels, as shown by Fonseca et al.[25] This implies that the numerical error varies linearly with Δt and quadratically with $1/N$. Assuming that other parameters have a weak influence on the absolute numerical error, defined in terms of Γ_w, Fonseca et al.[25] show that the algorithm converges and that numerical errors of the order of 10^{-4} (or lower) are obtained with $\Delta t = 0.01$ and $N = 150$. We use these values for all runs presented next.

The code is also validated for three flows. First, we remove the ground plane by letting h_g go to a large volume and perform the simulation of a 0–5 deg step change in the angle of attack for a NACA 0012 airfoil immersed in a uniform flow. As the simulation evolves in time, a starting vortex is formed, and the airfoil lift coefficient tends to the steady flow value for $\alpha = 5$ deg, comparing very well to results obtained by Vezza and Galbraith.[27] Second, we again remove the ground plane and simulate the interaction of a NACA 0012 airfoil set at zero angle of attack with a two-dimensional point vortex that passes over the airfoil. Two cases are considered: In the first, the vortex has dimensionless strength $\Gamma_v = -0.15$ and release point at $x_{v0} = -3.33$ and $y_{v0} = 0.24$; in the second, $\Gamma_v = 0.16$ with release point at $x_{v0} = -3.33$ and $y_{v0} = 0.19$. These are the values used in experiments carried out by Straus et al.[11] for a Reynolds number of 3.75×10^5. Again the results match the simulations of Fonseca et al.[25] as h_g goes to a large volume, which, in turn, compares well with the experiments. Finally, we remove the vortex and perform several calculations for a family of symmetrical four-digit NACA airfoils set at different angles of attack in ground effect. The results compare well to those of Widnall and Barrows[17] and present the same physical behavior as obtained by Coulliette and Plotkin[20] for a Joukowsky airfoil.

AVIG

The interaction of an oncoming two-dimensional (main) vortex with an airfoil immersed in a uniform flow in the presence of a ground plane comprises three simultaneous interactions: AVI, AGI, and the VGI. When it is assumed that viscous and compressibility effects can be neglected and that flow separation does not occur, the degree of interaction of each one of these three flows depends on a particular set of parameters. The unsteady AVI flow is affected by the aerofoil angle of attack and geometry (profile and thickness-to-chord and camber-to-chord ratios), the vortex strength, the vortex direction of rotation, and the vertical distance between the airfoil and the vortex. On the other hand, the properties of the steady flow around an airfoil in ground effect depend on the chord-to-wall clearance ratio, in addition to the aerofoil angle of attack and geometry. For the VGI flow, the unsteady motion of a vortex above an infinite plane wall is influenced mainly by the vortex strength, the vortex direction of rotation, and vortex height above the ground. As a consequence, each flow has different characteristics.

The AVI flow is characterized by a strong variation of the airfoil loading with time. As the vortex moves past the airfoil from far upstream following a local streamline, the pressure distribution and the forces on the airfoil change with time. For negative values of the vortex strength, the vortex induces a counterclockwise rotating flow that adds up to the freestream flow. When the vortex is upstream, it produces a local positive angle of attack on the airfoil, creating a positive lift that increases and reaches a maximum as the vortex approaches the vicinity of the leading edge. As the vortex gets past the airfoil leading edge, the local angle of attack is still positive in the trailing-edge region, but it is negative in the leading-edge region. The lift coefficient then starts to decrease at a high rate of change and reaches a minimum when the vortex is near the trailing edge. Finally, when the vortex is downstream of the trailing edge, the negative values of the lift coefficient increase again. For positive values of the vortex strength, the temporal variation of the lift coefficient reverses sign. In both situations, the quasi-steady and unsteady components of the aerodynamic forces are of the same order of magnitude. The degree of interaction can be measured through an appropriate dimensionless number. Based on the work of Bodstein et al.,[28] Fonseca et al.[25] have shown that the influences of the vortex strength and the distance between the airfoil and the vortex can be inferred by defining a nondimensional interaction parameter K according to

$$K \equiv \Gamma / U_\infty H = \Gamma_v / h_v \tag{25a}$$

where $h_v \equiv H/c$. Alternatively, a second nondimensional parameter, called the apparent interaction parameter K_a, can be defined as

$$K_a \equiv \Gamma_v / y_{v0} \tag{25b}$$

Both parameters, K and K_a, can be interpreted as the ratio of the longitudinal velocity induced by the vortex to the freestream speed, and they indicate that the interaction between the airfoil and the vortex becomes strong for high values of Γ_v and/or low values of h_v (or y_{v0}). Although K provides a measure of the actual degree of interaction, h_v is not known in advance, and the problem must be solved before K can be evaluated. On the other hand, the parameter K_a can be calculated without solving the problem. Note that the model developed here furnishes good results as long as the vortex does not intercept the airfoil, which happens when h_v (or y_{v0}) tends to zero, and therefore, K (or K_a) tends to infinity. In this case, the viscous vortex core in a real flow comes in direct contact with the airfoil's boundary layer, and a strong viscous interaction takes place, where the vortex core gets distorted and breaks up into two pieces, one that moves along the airfoil's upper surface and another that moves along the airfoil's lower surface. Vortex core distortion has been studied by Lee and Smith,[7] without considering the airfoil's boundary-layer effect. Interaction of this type is not accounted for in our model.

In the absence of a convecting vortex, the inviscid, incompressible flow of a two-dimensional airfoil close to an infinite wall located a distance $h_g \equiv h/c$ below the airfoil leading edge is steady, and it depends on h_g, α, and the airfoil thickness ε. The airfoil camber just adds a local angle of attack and a resulting extra lift, as shown by Coulliette and Plotkin.[20] Physically, the AGI flow generates suction in the region between the airfoil and the wall. On a symmetrical airfoil, the combined action of the airfoil thickness and the presence of the wall reduces the area underneath the airfoil, which causes the flow to accelerate, the streamlines to approach each other, and the pressure to reduce. In other words, the ground effect increases as ε increases, for a fixed airfoil height, or as h_g decreases, for a fixed ε. If a symmetrical airfoil is placed in ground effect and set at a low positive value of the angle of attack, the lift coefficient presents a different behavior. When $h_g \to \infty$, the suction effect caused by the ground goes to zero, and the lift coefficient tends to a value slightly less than the value for the steady flow around an airfoil at incidence immersed in an unbounded fluid. As h_g is reduced from infinity, the value of C_l increases, reaches a maximum, and then decreases. Whereas the ground effect, considered in isolation, causes suction underneath the airfoil, the sole effect of the angle of attack is to increase the lift coefficient as the ground is brought closer to the airfoil. This result is shown analytically for a zero-thickness flat plate at incidence (and for a parabolic-arc airfoil at zero incidence) by Coulliette and Plotkin[20]. Therefore, for a nonzero thickness symmetrical airfoil, there is competition between the effect of the angle of attack that increases the lift, for fixed h_g, and the suction effect that decreases the lift as $h_g \to 0$. In summary, the angle of attack effect becomes important as h_g is decreased from a large value and C_l goes up. Eventually, the suction effect becomes stronger, and the value of the lift coefficient goes down to a negative value, with a point of maximum being reached in between. This behavior is also observed in our calculations and in the ones reported by Coulliette and Plotkin (Fig. 11, Ref. 20) for a Joukowsky airfoil.

For the VGI flow, the third flow that comprises the AVIG flow, a two-dimensional vortex moves above an infinite plane wall. For an incompressible inviscid flow, the vortex generates a suction peak underneath its center, bounded by two regions of high pressure, one upstream and the other downstream of the peak. The analytical solution to this flow, expressed from a reference frame fixed to the vortex center, can be found by Milne-Thomson.[21] This pressure distribution

moves with the vortex and causes regions of favorable, as well as adverse, pressure gradients. The degree of interaction depends on the value of the vortex strength and the height of the vortex above the ground. These parameters can be reduced to a single interaction parameter, namely, $\Gamma/(U_\infty h_v)$. For high values of this parameter, the interaction is strong. If the value of the interaction parameter is large in a viscous flow, the boundary layer on the ground would suffer more severe pressure gradient effects, and separation might occur in regions of adverse pressure gradients. Doligalsky et al.[22] discuss in detail the flow physics and many numerical solutions available in the literature for viscous vortex interactions with walls.

The AVIG flow encompasses simultaneously the three flows described and, therefore, depends on the entire set of parameters that influence these three flows. Again, we consider the AVIG flow to be two-dimensional, incompressible, inviscid, unsteady, and without the occurrence of separation. Only one airfoil is chosen, the symmetrical NACA 0012, because the thickness ratio only enhances the suction effect caused by the ground plane on the airfoil lift coefficient. Because the vortex is closer to the airfoil than to the ground, the vortex–ground plane interaction parameter plays a less important role than the AVI parameter K (or K_a). Hence, the parameters that are most important in the flow are K (or K_a), h_g, and α. In the simulations to come, we adopt the same values of the vortex strength and release points used in the simulations of Fonseca et al.[25] Two cases are considered. In the first, the vortex has dimensionless strength $\Gamma_v = -0.15$ and release point at $x_{v0} = -3.33$ and $y_{v0} = 0.24$. In the second, $\Gamma_v = 0.16$ with release point at $x_{v0} = -3.33$ and $y_{v0} = 0.19$. With these coordinates and values of the vortex strength, in addition to the numerical values of h_v obtained from the simulations, Eqs. (25) furnish $K = -0.63$ and $K_a = -0.63$ for $\Gamma_v = -0.15$ and $K = 1.23$ and $K_a = 0.84$ for $\Gamma_v = 0.16$. It is clear that the case where the vortex rotates in the clockwise direction corresponds to the strongest interaction case.

We begin by considering the effect of the flow on the airfoil. Figures 2 and 3 present the temporal variation of the lift and pitching moment coefficients, respectively, on a NACA 0012 airfoil set at zero angle of attack, for $\Gamma = -0.15$ and $\Gamma = 0.16$, having the chord-to-wall clearance ratio as a parameter. In Fig. 2a, the C_l curve with the highest values corresponds to the pure AVI flow ($h_g \to \infty$) and shows a history that matches the results obtained by Fonseca et al.[25] In this case, the lift coefficient is positive when the vortex is far upstream of the leading edge, and it increases as the vortex approaches the airfoil, reaching a maximum value near the leading edge. On the other hand, the pitching moment coefficient about the leading edge is negative and decreases with time, reaching a minimum near the leading edge (Fig. 3a). As the vortex moves above the airfoil, the lift coefficient goes down and reaches a minimum by the trailing-edge region, whereas the pitching moment coefficient increases and reaches a maximum, as discussed earlier for the AVI flow. For $\Gamma = 0.16$, the direction of the vortex rotation is reversed. As shown in Figs. 2b and 3b, the temporal variation of C_l and C_m for $h_g \to \infty$ changes sign and presents a stronger C_l variation than the earlier case near the trailing edge, which is a consequence of the stronger interaction between the vortex, the airfoil, and the wake. (K and K_a are higher in this case.) As h_g decreases, the suction effect due to the presence of the wall moves the C_l curve down and the C_m curve up for the $\Gamma_v = -0.15$ ($K_a = -0.63$) case. These results show that, for this value of Γ_v, the suction effect dominates. However, when $\Gamma_v = 0.16$ ($K_a = 0.84$), the interaction is stronger, and despite the qualitative similarity of the flows with and without the ground plane nearby, the presence of the wall in this case promotes competition among the lifting effect caused by the nonlinear

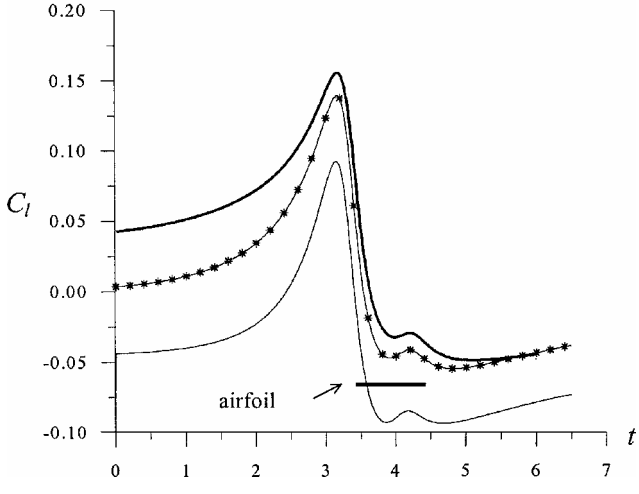

a) $\Gamma_v = -0.15$

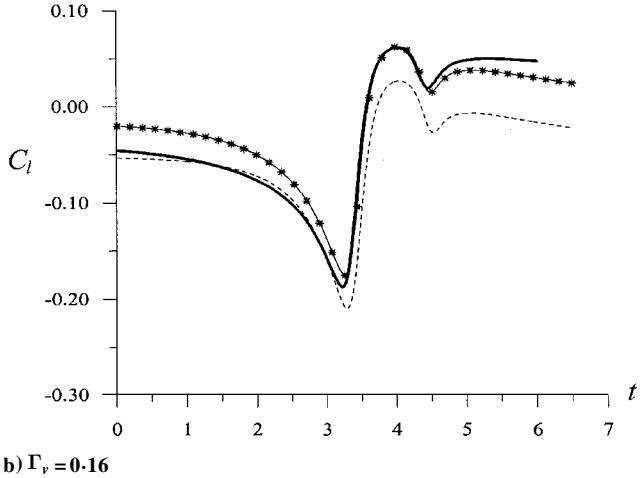

b) $\Gamma_v = 0.16$

Fig. 2 Effect of h_g on the temporal variation of C_l, NACA 0012, and $\alpha = 0$: ——, $h_g \to \infty$; ∗, $h_g = 1.0$; and - - - -, $h_g = 0.5$.

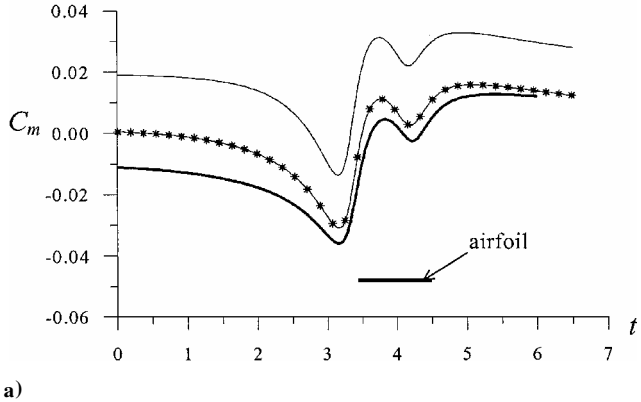

a)

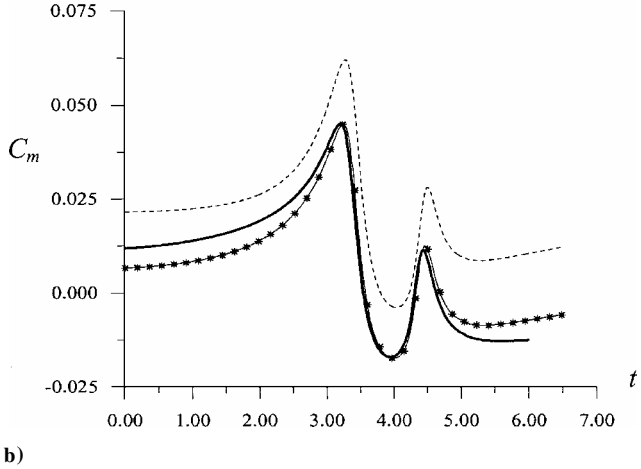

b)

Fig. 3 Effect of h_g on the temporal variation of C_m, NACA 0012, and $\alpha = 0$: a) $\Gamma_v = -0.15$: ——, $h_g = 0.5$; ∗, $h_g = 1$; and ——, $h_g \to \infty$ and b) $\Gamma_v = 0.16$: ——, $h_g \to \infty$; ∗, $h_g = 1$; and - - - -, $h_g = 0.5$.

vortex trajectory and the suction effects originating from the airfoil thickness and clearance to the wall, having the nonlinear wake interaction in the background. Because of the stronger vortex-wake interaction, the total effect is that C_l and C_m do not increase or decrease monotonically with h_g. As the results attest, reducing the value of h_g causes the C_l curve on the airfoil to move up (and the C_m curve to move down) when $h_g = 1.0$. For $h_g = 0.5$, the suction effect dominates again, and the C_l values are lower than its values without the wall, whereas the C_m values are higher. These results for the airfoil loading history shows the interesting nonlinear behavior of the AVIG flow due to the nonlinear vortex trajectory and wake interaction effects, as well as the competition between the vortex lifting and ground suction effects. The intensity of the interaction, quantified by K_a, and the vortex direction of rotation have a direct influence on the flow evolution. To isolate the effect of the angle of attack, Fig. 4 presents results for a NACA 0012 airfoil set at two different values of α, for $\Gamma_v = -0.15$ and $h_g = 0.5$. As can be seen, Fig. 4 shows that an increase in the airfoil's angle of attack to 1 and 5 deg causes an increase in the variation of the absolute values of the lift and pitching moment coefficients with time, as shown in Figs. 4a and 4b, respectively.

We now turn our attention to the effect that the AVI-ground plane interaction has on the ground pressure distribution. Figure 5 shows the pressure coefficient as a function of the x distance along the ground for the same NACA 0012 airfoil set at zero incidence interacting with the counterclockwise rotating vortex ($\Gamma_v = -0.15$). The

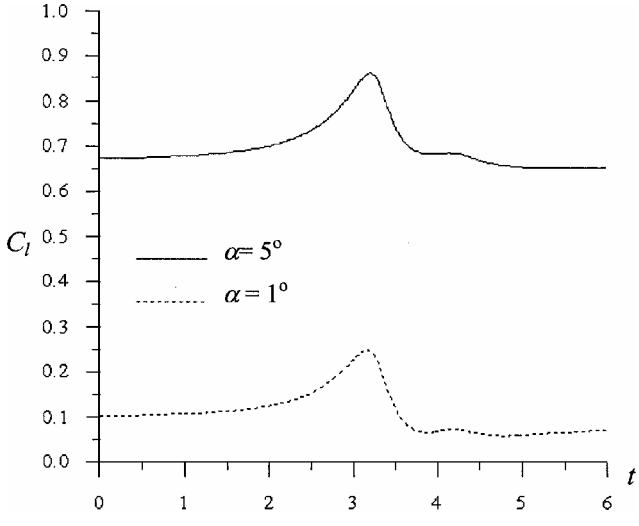

a) Lift coefficient

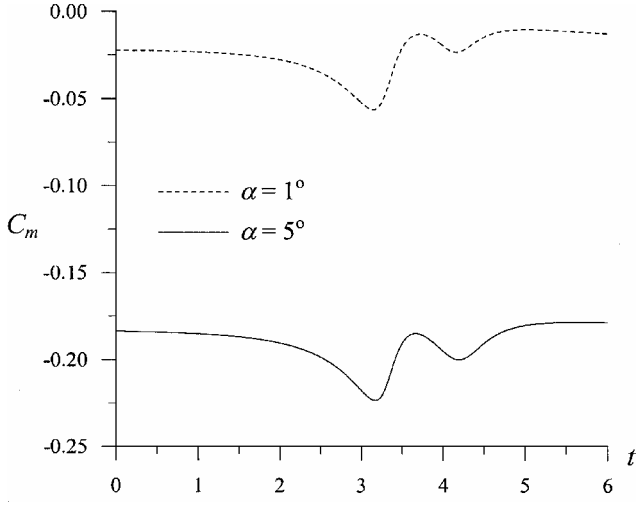

b) Pitching moment coefficient

Fig. 4 Effect of α on the temporal variation of C_l and C_m, $\Gamma_v = -0.15$, NACA 0012, and $h_g = 0.5$.

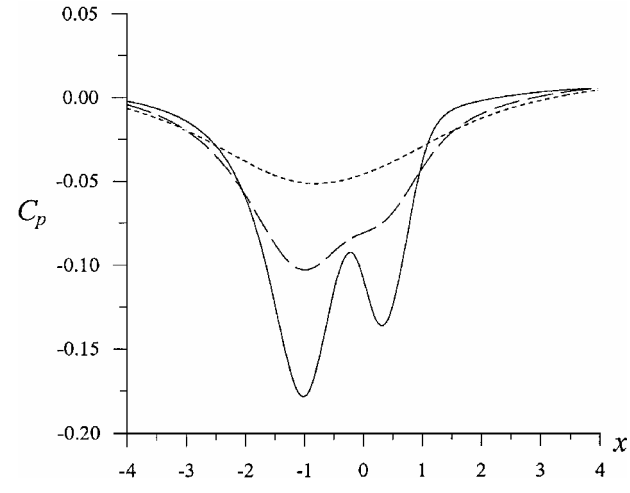

a)

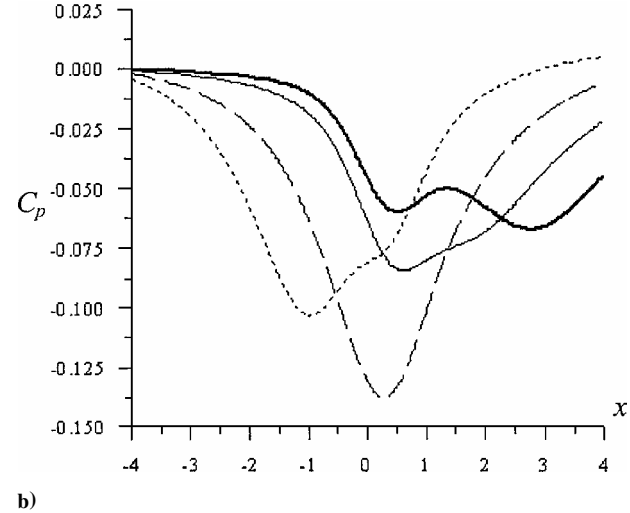

b)

Fig. 5 Pressure coefficient distribution on the ground, NACA 0012, $\Gamma_v = -0.15$, and $\alpha = 0$: a) effect of h_g, $x_v = -1.0$: - - - -, $h_g = 2.0$; – – –, $h_g = 1.0$; and ——, $h_g = 0.5$ and b) effect of the vortex position, $h_g = 1$: - - - -, $x_v = -1.0$; – – –, $x_v = 0$; ——, $x_v = 1.0$; and ▬▬, $x_v = 2.0$.

effect of the chord-to-wall clearance ratio on the ground when the vortex is at the position $x_v = -1.0$, shown in Fig. 5a, is to create two suction peaks, one due to the main vortex and the other due to the airfoil. Whereas the main vortex contributes to accelerate the flow underneath it, the airfoil also accelerates the flow underneath it because of its thickness, decreasing the pressure in both cases. For the values used in the computations, the vortex effect is greater than the airfoil thickness effect, as clearly shown for $h_g = 0.5$. These peaks merge and decrease their values for the larger values of h_g. Also note from Fig. 5b the evolution of the suction peaks, as the vortex moves past the airfoil and the chord-to-wall clearance ratio is kept constant and equal to $h_g = 1.0$. When the vortex is above the airfoil, both suction peaks add up to form a very large negative peak. The adverse pressure gradient downstream of the peak is likely to produce separation on the ground, with the generation of a secondary vortex that would complicate the real flow even more. As the vortex gets past the airfoil, the vortex and the airfoil suction peaks can again be distinguished. When the vortex direction of rotation is reversed, the opposite trends are observed (Fig. 6). Because the vortex rotates in the clockwise direction, the velocity it induces is subtracted from the remaining of the flow, which decelerates the total flow and increases the pressure on the ground. This is the reason why Fig. 6a shows first a large positive peak on the ground right underneath the vortex (near the leading edge), followed by a negative peak due to the airfoil's suction effect. These peaks increase as the airfoil is brought closer to the ground. Snapshots of the temporal evolution of the pressure

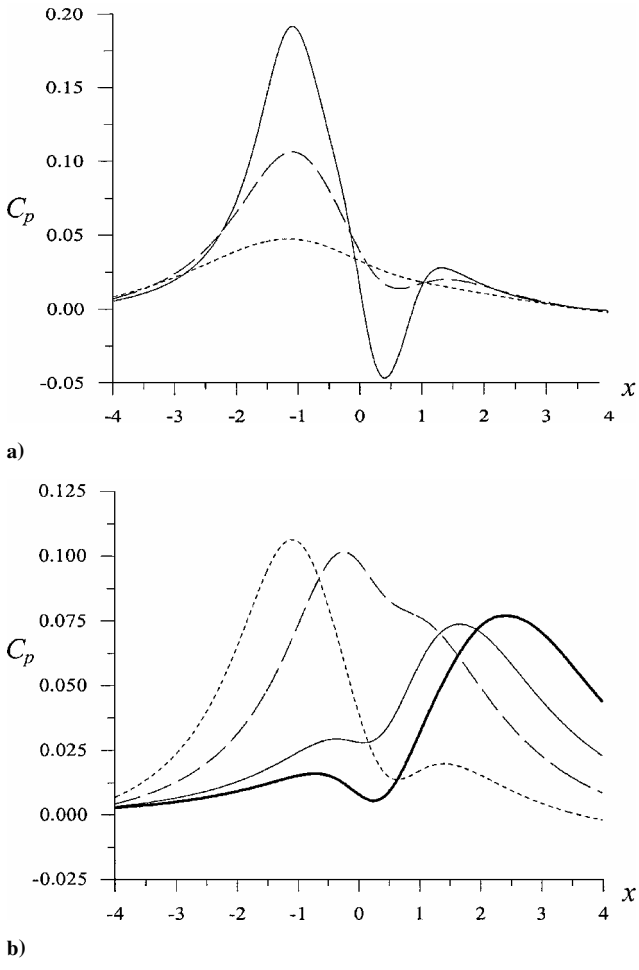

Fig. 6 Pressure coefficient distribution on the ground, NACA 0012, $\Gamma_v = 0.16$, and $\alpha = 0$: a) effect of h_g, $x_v = -1.0$: ----, $h_g = 2.0$; – – –, $h_g = 1.0$; and ——, $h_g = 0.5$ and b) effect of the vortex position, $h_g = 1.0$: ----, $x_v = -1.0$; – – –, $x_v = 0$; ——, $x_v = 1.0$; and ▬, $x_v = 2.0$.

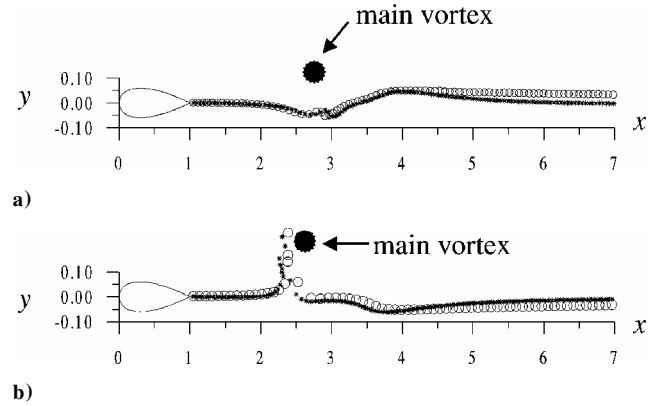

Fig. 7 Influence of the ground on the wake, $t = 6$ and $\alpha = 0$ deg: a) $\Gamma_v = -0.15$: ⁎, $h_g = 0.5$ and ○, $h_g = 10$ and b) $\Gamma_v = 0.16$.

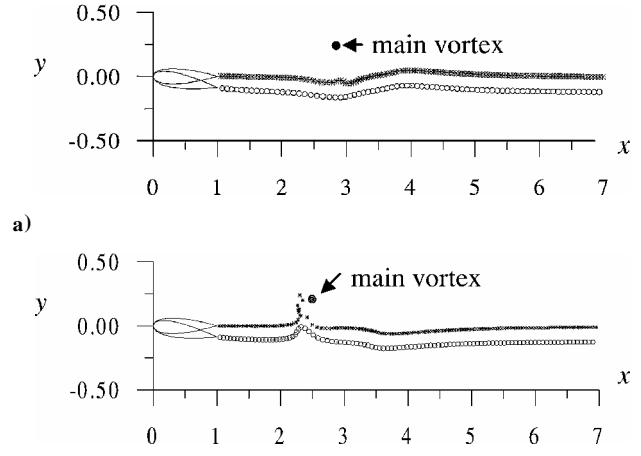

Fig. 8 Influence of the angle of attack on the AVIG flow, $t = 6$, and $h_g = 0.5$: a) $\Gamma_v = -0.15$: ⁎, $\alpha = 0$ deg and ○, $\alpha = 5$ deg and b) $\Gamma_v = 0.16$.

coefficient as the vortex moves past the airfoil (Fig. 6b) show that the positive peak due to the vortex dominates and moves with the vortex, because the vortex effect in our computations is stronger than the airfoil's suction effect. These results for the pressure coefficient distribution on the ground enlighten us for the possible occurrence of flow separation, which would strongly affect the flow as a whole.

Finally, the wake development and its interaction with the main vortex can be seen in Fig. 7 with and without the ground effect, at $t = 6$, for both directions of the vortex strength. We clearly see that the counterclockwise rotating vortex induces a downward motion on the wake upstream of the vortex and an upward motion downstream of the vortex. In addition, the effect of the ground plane is to bring the wake closer to the ground because of the low pressure in this region, as indicated by the large suction peak on the wall created by the vortex (Fig. 5). The clockwise rotating vortex, on the other hand, induces an upward wake motion upstream of the vortex, which lifts up the wake vortices and causes a very strong interaction in a region of high pressure, as it can be seen from the ground plane pressure distribution (Fig. 6b). As Fig. 7 shows, the vortex effect is more important than the ground effect on the wake development because the wake configuration changes only slightly for $h_g = 0.5$ and $h_g = 10$. With the airfoil set at a 5-deg angle of attack in ground effect, the airfoil lift is positive (Fig. 4), and its circulation is clockwise, which induces a downward motion on the wake (Fig. 8) close to the trailing edge of the airfoil. Note also that, because the airfoil is rotated by its leading edge when set at a positive angle of attack, the airfoil's trailing edge moves downward, changing the release point of the wake vortices. Both effects contribute to weaken the vortex-wake interaction and to smooth out the wake trajectory, as shown in Fig. 8a, at $t = 6$. Figure 8b shows essentially the same effects on the wake configuration for the clockwise rotating vortex, at time $t = 6$, because the airfoil circulation and the new release point of the wake vortices cause the wake to be lower than the 0-deg angle-of-attack wake. As a consequence, the vortex–wake interaction decreases and smoothes out the peak of the lifted portion of the wake trajectory. Clearly our vorticity shedding mechanism with a discrete vortex representation of the wake is responsible for capturing the nonlinear effect between the vortex and the wake, mainly when the interaction is strong. These results point out the importance of modeling correctly the shedding of vorticity in a real flow.

Conclusions

A numerical inviscid vortex model is used to predict the aerodynamics of a two-dimensional AVI in the presence of a ground plane. The model employs a panel method with a linear piecewise-continuous vorticity distribution to calculate the airfoil contribution to the potential flow and a point vortex to model the main vortex that interacts with the airfoil. An unsteady Kutta condition is implemented to generate point vortices in the wake, and the ground effect is taken into account by the method of images. The convective motion of each vortex is calculated using a time-marching scheme. After code validation tests, the results show important features of the interaction among the airfoil, the vortex, and the ground plane, and the following conclusions can be drawn.

1) The airfoil in ground effect suffers a strong temporal variation of its loading as the vortex moves past the airfoil from far upstream. The distance between the airfoil and the vortex, the direction of the vortex rotation, the value of the vortex strength, and the chord-to-wall clearance ratio are extremely important in determining the degree of interaction.

2) The airfoil thickness and chord-to-wall clearance ratio effects add up to generate suction beneath the airfoil and to decrease the lift coefficient, whereas a positive airfoil angle of attack increases its lift coefficient. The competition among these effects determines the loading on the airfoil.

3) The vortex induces a time-dependent local angle of attack on the airfoil that adds up to the airfoil geometric angle of attack and generates a time-varying lift effect, whereas the airfoil thickness and ground effect cause suction. Competition among these effects is established during the motion.

4) The ground is subject to a strong pressure variation, depending on the strength and direction of vortex rotation and its proximity to the vortex and the airfoil. The occurrence of adverse pressure gradient may cause separation on the ground.

5) The ground effect and the airfoil angle of attack affect strongly the trajectory of the wake vortices and its nonlinear interaction with the main vortex, which has a definite effect on the temporal wake evolution and the flow as a whole.

Our model, although simple, is able to model all of the main inviscid features that take place in the AVI in the presence of a ground plane. To predict the possible occurrence of flow separation on the airfoil surface and on the ground plane, it is necessary to model viscous effects. This comprises the next step in the modeling of such a complex flow.

Acknowledgments

The authors would like to acknowledge CAPES, for the M.Sc. scholarship granted to G. F. Fonseca, FAPEMIG, under Grant TEC-1565/97, and the Brazilian National Research Council for the financial support of this project through grants AI 143041/97-5, AI 551364/02-5, and APQ 474904/01-6.

References

[1]Hefner, J. N., Anders, J. B., and Bushnell, D. M., "Alteration of Outer Flow Structures for Turbulent Drag Reduction," AIAA Paper 830-0293, June 1983.

[2]Savill, A. M., and Mumford, J. C., "Manipulation of Turbulent Boundary Layers by Outer-Layer Devices; Skin Friction and Flow-Visualisation Results," *Journal of Fluid Mechanics*, Vol. 191, 1988, pp. 389–418.

[3]Gebert, G. A., and Atassi, H. M., "Unsteady Vortical Disturbances Around a Thin Airfoil in the Presence of a Wall," *AIAA Journal*, Vol. 27, No. 10, 1989, pp. 1448–1451.

[4]Im, Y.-H., and Chang, K.-S., "Unsteady Aerodynamics of a Wing-in-Ground-Effect Airfoil Flying over a Wavy Wall," *Journal of Aircraft*, Vol. 37, No. 4, 2000, pp. 690–696.

[5]Panaras, A. G., "Numerical Modeling of the Vortex/Airfoil Interaction," *AIAA Journal*, Vol. 25, No. 1, 1987, pp. 5–11.

[6]Poling, D. R., Dadone, L., and Telionis, D. P., "Blade–Vortex Interaction," *AIAA Journal*, Vol. 27, No. 6, 1989, pp. 694–699.

[7]Lee, D. J., and Smith, C. A., "Effect of Vortex Core Distortion on Blade–Vortex Interaction," *AIAA Journal*, Vol. 29, No. 9, 1991, pp. 1355–1362.

[8]Srinivasan, G. R., and McCroskey, W. J., "Euler Calculations of Unsteady Interaction of Advancing Rotor with a Line Vortex," *AIAA Journal*, Vol. 31, No. 9, 1993, pp. 1659–1666.

[9]Rai, M. M., "Navier–Stokes Simulations of Blade–Vortex Interaction Using High-Order Accurate Upwind Schemes," AIAA Paper 87-0543, Nov. 1987.

[10]Seath, D. D., Kim, J.-M., and Wilson, D. R., "Investigation of Parallel Blade–Vortex Interaction at Low Speed," *Journal of Aircraft*, Vol. 26, No. 4, 1989, pp. 328–333.

[11]Straus, J., Renzoni, P., and Mayle, R. E., "Airfoil Pressure Measurements During a Blade Vortex Interaction and a Comparison with Theory," *AIAA Journal*, Vol. 28, No. 2, 1990, pp. 222–228.

[12]Chen, J. M., and Chang, D.-M., "Unsteady Pressure Measurements for Parallel Vortex–Airfoil Interaction at Low Speed," *Journal of Aircraft*, Vol. 34, No. 3, 1997, pp. 330–336.

[13]McCune, J. E., and Tavares, T. S., "Perspective: Unsteady Wing Theory—The Karman/Sears Legacy," *Journal of Fluids Engineering*, Vol. 115, Dec. 1993, pp. 548–560.

[14]Mook, D. T., and Dong, B., "Perspective: Numerical Simulations of Wakes and Blade–Vortex Interaction," *Journal of Fluids Engineering*, Vol. 116, March 1994, pp. 5–21.

[15]Havelock, T. H., "The Lift and Moment on a Flat Plate in a Stream of Finite Width," *Proceedings of the Royal Society of London*, Series A: *Mathematical and Physical Sciences*, Vol. 166, 1938, pp. 178–196.

[16]Green, A. E., "The Two-Dimensional Airfoil in a Bounded Stream," *Quarterly Journal of Mathematics*," Vol. 18, 1947, pp. 167–177.

[17]Widnall, S. E., and Barrows, T. M., "An Analytic Solution for Two- and Three-Dimensional Wings in Ground Effect," *Journal of Fluid Mechanics*, Vol. 41, Pt. 4, 1970, pp. 769–792.

[18]Plotkin, A., and Kennell, C. G., "Thickness-Induced Lift on a Thin Airfoil in Ground Effect," *AIAA Journal*, Vol. 19, No. 11, 1981, pp. 1484–1486.

[19]Dragos, L., "Numerical Solution of the Equation for a Thin Airfoil in Ground Effect," *AIAA Journal*, Vol. 28, No. 12, 1990, pp. 2132–2134.

[20]Coulliette, C., and Plotkin, A., "Airfoil Ground Effect Revisited," *Aeronautical Journal*, Feb. 1996, pp. 65–74.

[21]Milne-Thomson, L. M., *Theoretical Hydrodynamics*, MacMillan, New York, 1968, pp. 360, 361.

[22]Doligalski, T. L., Smith, C. R., and Walker, J. D. A., "Vortex Interactions with Walls," *Annual Review of Fluid Mechanics*, Vol. 26, 1994, pp. 573–616.

[23]Dowling, A. P., "The Effect of Large-Eddy Breakup Devices on Oncoming Vorticity," *Journal of Fluid Mechanics*, Vol. 160, 1985, pp. 447–463.

[24]Balakumar, P., and Widnall, S. E., "Application of Unsteady Aerodynamics to Large-Eddy Breakup Devices in a Turbulent Flow," *Physics of Fluids*, Vol. 29, June 1987, pp. 1779–1787.

[25]Fonseca, G. F., Bodstein, G. C. R., and Hirata, M. H., "A Numerical Inviscid Vortex Model Applied to Parallel Blade–Vortex Interaction," *Journal of the Brazilian Society of Mechanical Sciences*, Vol. 19, No. 3, 1997, pp. 341–356.

[26]Katz, J., and Plotkin, A., *Low Speed Aerodynamics*, 2nd ed., Cambridge Univ. Press, 2001, Cambridge, England, U.K., pp. 303–306.

[27]Vezza, M., and Galbraith, R. A. M., "A Method for Predicting Unsteady Potential Flow about an Aerofoil," *International Journal for Numerical Methods in Fluids*, Vol. 5, 1985, pp. 347–356.

[28]Bodstein, G. C. R., George, A. R., and Hui, C.-Y., "The Three-Dimensional Interaction of a Streamwise Vortex with a Large-Chord Lifting Surface: Theory and Experiment," *Journal of Fluid Mechanics*, Vol. 322, 1996, pp. 51–79.